
Mitigation of Cross-Beam Energy Transfer: Implications of Two-State Optical Zooming on OMEGA

Introduction

Two approaches to inertial confinement fusion (ICF)¹ employ megajoule-class laser systems^{2,3} to compress a fusion capsule to thermonuclear burn conditions. For the indirect-drive approach,⁴ the laser beams heat a radiation cavity, crossing in a low-density plasma on their path to the cavity wall; for the direct-drive approach,^{5,6} the laser beams directly illuminate the fusion capsule and laser rays cross in higher-density coronal plasma. In both ignition schemes, crossing laser beams can excite ion-acoustic waves that facilitate the energy transfer away from regions of interest.^{7–11}

For indirect-drive-ignition experiments, cross-beam energy transfer (CBET) removes significant energy from the beams directed near the equator of the capsule, compromising the symmetry of the implosion.¹⁰ By changing the relative frequency between the laser beams, CBET has been mitigated and frequency shifts are now used to control the symmetry of the fusion capsule at the National Ignition Facility.^{12–14}

Direct-drive implosions on the OMEGA laser¹⁵ use three ~100-ps-long laser pulses (“pickets”) to launch shocks into the target, setting the implosion onto a low adiabat.⁶ These picket pulses are followed by a high-intensity drive pulse that compresses the fuel. During the drive, experiments have shown that CBET can reduce the hydrodynamic coupling by linking the scattered-light spectra to a lack of energy penetrating to the critical surface.^{16,17} Laser light in the edge of the laser beams propagating past the target beats with the incident laser light from the opposing beams and excites ion-acoustic waves. The enhanced ion-acoustic waves scatter light primarily from the central rays of the incident laser beams to the outgoing rays.

Studies have shown that reducing the diameter of the laser beams by 30% can restore 70% of the energy lost to CBET at the cost of reduced hydrodynamic stability.¹⁸ Simulations indicate no deleterious effects on hydrodynamic stability when the laser-beam diameters are reduced after a significant thermal conduction zone has been generated (two-state zooming). Zooming is predicted to increase the hydrodynamic efficiency,

allowing OMEGA to drive more-stable implosions at higher velocities and ignition-relevant, one-dimensional (1-D) yields.¹⁹

Potential schemes to achieve zooming of the focal spot on target involve modifications to the spatial coherence of the laser that cause broadening in the far field of the beam.²⁰ Two primary options for implementing zooming on OMEGA were investigated: (1) time-dependent phase conversion and (2) increased deflection from two-dimensional (2-D) smoothing by spectral dispersion (SSD).²¹ The most-practical method for implementing zooming on OMEGA appears to be time-dependent phase conversion. It is predicted to increase the absorption and allow for designs that include 9.5 μm of carbon–deuterium (CD) polymer and 66- μm -thick deuterium–tritium (DT) shells to be driven at $\sim 3.2 \times 10^7$ cm/s and produce ignition-scalable 1-D yields of 7.8×10^{13} —a factor of ~ 2.5 larger yields than produced without zooming. Implementing time-dependent phase conversion on OMEGA will require zooming phase plates (ZPP’s) and co-propagating dual-driver lines.

1. Zooming Phase Plates

A new phase-plate design, referred to as a zooming phase plate (ZPP), in conjunction with a time-dependent near-field profile will produce a larger laser spot during the pickets and a smaller laser spot during the main drive. The ZPP would contain a radial transition where the central area produces a larger, low-order super-Gaussian focal spot, while the outer area produces a smaller, high-order super-Gaussian focal spot. This configuration requires a smaller-diameter beam during the pickets and a mid-section cutout of the near field during the drive pulse, as shown in Fig. 133.40(a). OMEGA operates near its maximum stored-energy capacity, requiring that the diameter of the laser beams during the drive fill the complete aperture [Fig. 133.40(b)]. The OMEGA-limited near-field profiles combined with the proposed ZPP’s produce laser spots with low-intensity wings.

2. Co-Propagating Dual-Driver Lines

To produce the required two-state near-field profile, a co-propagating dual-driver configuration is required. The picket

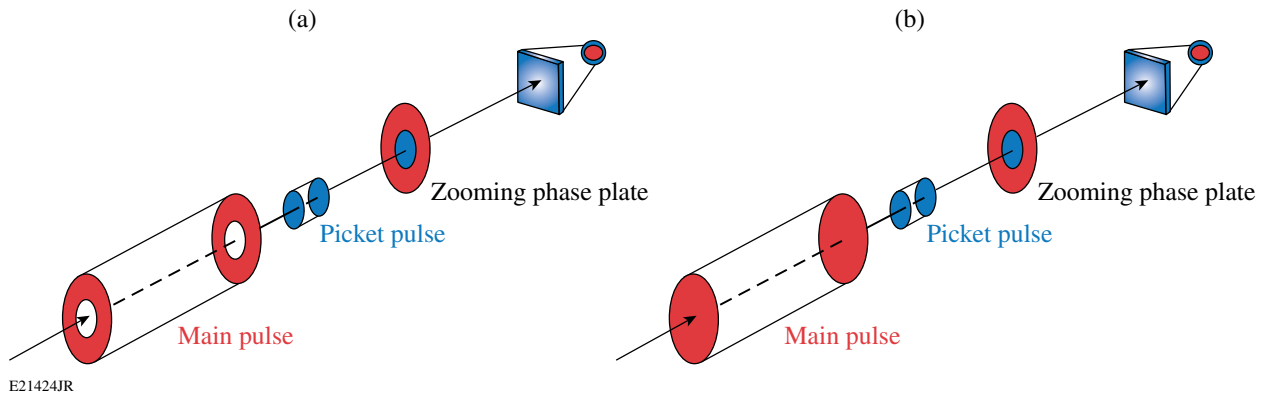


Figure 133.40

The (a) optimum and (b) OMEGA-limited near-field profiles for implementing radially varying ZPP's to produce large-diameter laser spots during the pickets (blue) and small-diameter spots during the drive pulse (red).

driver with SSD would pass through an apodizer, forming a beam of half the standard diameter. The second main-pulse driver would propagate without SSD through its own apodizer, forming a full-diameter beam [Fig. 133.40(b)].

Introducing a dual-driver configuration will provide the following:

- a 14-cm-diam beam during the pickets ($1.5\text{-}\text{\AA} \times 3\text{-}\text{\AA}$ SSD) and a full-aperture, 28-cm-diam beam (no SSD) during the main drive;
- an $\sim 10\%$ increase in on-target energy as a result of better frequency-conversion efficiency; and
- a proof-of-principle dynamic bandwidth reduction for the National Ignition Facility (NIF).

Implementing zooming using the proposed method presents two main concerns: (1) The small-diameter beams required during the pickets will increase intensity modulations in the imprint spectrum by a factor of 1.5 to 2. The impact of this increased imprint will be investigated but recent mitigation studies have demonstrated a factor-of-2 imprint reduction when using doped ablaters.^{22,23} (2) Zooming increases the single-beam intensities ($\sim 2\times$) during the drive. This may be above the backscatter intensity thresholds and lead to larger levels of hot electrons produced by two-plasmon decay.

This article is organized as follows: The target-physics implications of CBET and the initial results that are the foundation for a CBET mitigation scheme are described; a CBET mitigation scheme for direct-drive implosions, reviews of the physics considerations, and requirements for implementing this scheme on OMEGA are presented; proposed physics studies

to be completed prior to implementing the scheme are summarized; implementation of zooming on OMEGA is discussed; and the findings are summarized. An appendix presents an alternative concept for zooming (increased deflection from 2-D SSD) and the related calculations used to assess its feasibility.

Target Physics

1. Implications of Cross-Beam Energy Transfer in Direct Drive

The direct-drive approach to inertial confinement fusion requires that the laser beams efficiently deposit their energy in the coronal plasma where the energy is transported through the conduction zone to the ablation surface, producing the pressure that drives the implosion. This ablation pressure (P_a) determines the minimum laser energy required for ignition ($E_{\min} \propto P_a^{-2}$) (Ref. 24). Reducing the diameter of the laser beams increases the ablation pressure because it increases the energy in the central portions of the laser beams that propagate most normal to the target surface and deposit their energy closest to the ablation surface. This is balanced by the required increase in the diameter of the laser beams to minimize the illumination nonuniformities on target.

CBET is a mechanism that reduces the ablation pressure in direct-drive implosions.^{11,16–18} It reduces the incident energy in the central portion of the laser beams, making it possible for the incoming light to bypass the highest-absorption region near the critical surface (Fig. 133.41), significantly reducing the hydrodynamic efficiency.¹⁷ Laser light in the edge of the laser beams (\vec{k}_2) propagating past the target seeds stimulated Brillouin scattering (SBS) using light from the opposing laser beams (\vec{k}_1) and drives ion-acoustic waves (\vec{k}_a). The ion-acoustic waves scatter light primarily from the central rays of the incident laser beams to the lower-energy outgoing rays.

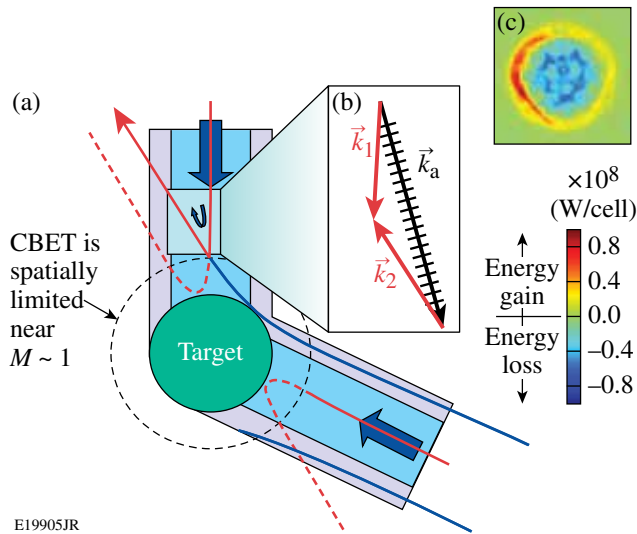


Figure 133.41

(a) Light rays propagating past the target (blue) interact with light rays in the central region of another beam (red). (b) The interacting light rays seed an ion-acoustic wave near the Mach-1 surface (dashed curves). The ion-acoustic wave scatters light before it can penetrate deep into the target. (c) A calculation of the total energy transferred (gain/lost) integrated along the path of a ray into and out of the target. The calculation shows that energy in the central rays propagating into the target is reduced by CBET, while the energy in the edges of the beam propagating away from the target is increased.²⁵

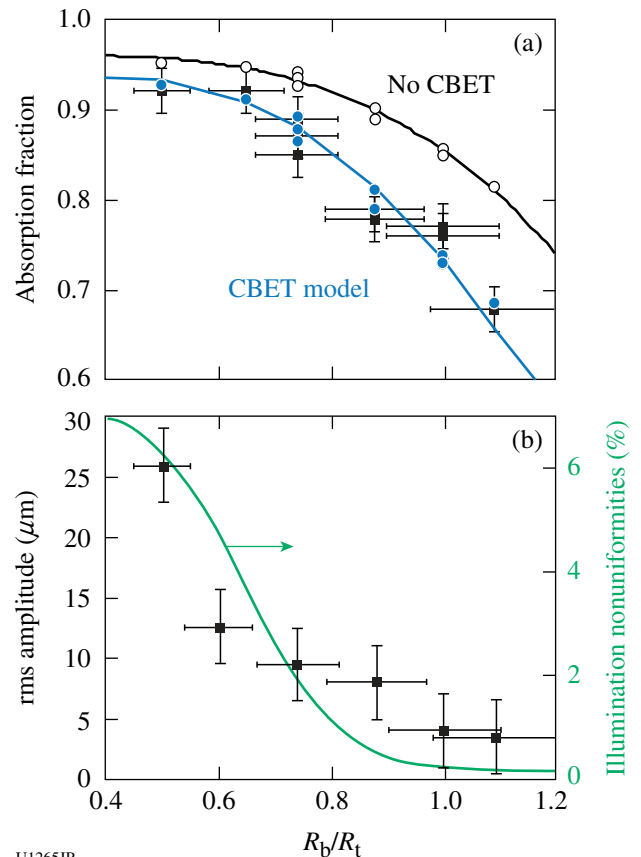
Simulations of direct-drive implosions using the 1-D radiation–hydrodynamics code *LILAC*²⁶ that include CBET modeling indicate that the ablation pressure is reduced by $\sim 40\%$, lowering the implosion velocity ($v_{\text{imp}} \propto P_a$), the hot-spot pressure ($P_{\text{hs}} \propto P_a^{1/3}$), the areal density ($\rho R \propto \sqrt{P_a}$), and negatively impacting the stability of the implosion as inferred from the in-flight aspect ratio (IFAR $\propto P_a^{-2/5}$) (Ref. 24). The loss in ablation pressure limits OMEGA cryogenic implosions, reducing the 1-D yield by nearly an order of magnitude.

The implosion velocity calculated for a 1.5-MJ, symmetric, direct-drive–ignition design⁶ is reduced from 4.0×10^7 to 3.3×10^7 cm/s (Ref. 19). CBET significantly increases the minimum energy required for ignition and 1-D simulations suggest that the ignition margin cannot be recovered by increasing the on-target laser energy while maintaining a constant overlapped intensity. Increasing the laser energy to account for the lost ablation pressure requires an increased laser-beam radius that results in longer scale lengths and increased CBET. The increased energy does not recover the loss in hot-spot pressure, suggesting that the implosions must be driven at higher velocities, further reducing their hydrodynamic stability.

2. Mitigation of Cross-Beam Energy Transfer (Zooming)

Experiments have demonstrated that reducing the laser-beam diameters with respect to the target diameter can reduce CBET at the cost of increased illumination nonuniformities (Fig. 133.42).¹⁸ To mitigate CBET and maintain sufficient illumination uniformity, a two-state zooming has been proposed.¹⁹ During the critical time for seeding nonuniformities, the radii of the laser beams R_b are equal to the target radius R_t ($R_b/R_t = 1$), minimizing the low-frequency laser imprint. Once a conduction zone is long enough to suitably smooth laser imprint, the diameters of the laser beams are reduced and CBET can be mitigated.

LILAC simulations show that implementing zooming by reducing the 95% encircled energy radii of the laser beams after the third picket from $R_b = 430 \mu\text{m}$ ($R_b/R_t = 1.0$) to $R_b = 365 \mu\text{m}$



U1265JR

Figure 133.42

The measured (a) absorbed light (squares) and (b) rms deviation from the average shell radius (squares, left axis), along with the calculated illumination nonuniformities (right axis) are plotted as functions of the ratio between the laser-beam and target radii, where R_b is the 95% encircled energy radius. The calculated absorption is shown in (a) for simulations with (blue solid circles) and without CBET modeling (open circles) for an overlapped intensity of 4.5×10^{14} W/cm² (Ref. 17).

($R_b/R_t = 0.85$) recovers 35% of the absorption lost to CBET and the implosion velocity for less-massive targets ($10 \mu\text{m}$ of CD + $44\text{-}\mu\text{m}$ -thick DT shells) reaches values of $3.7 \times 10^7 \text{ cm/s}$ [Fig. 133.43(a)]. Further reducing the radii of the laser beams to $R_b = 300 \mu\text{m}$ ($R_b/R_t = 0.7$) recovers 70% of the energy lost to

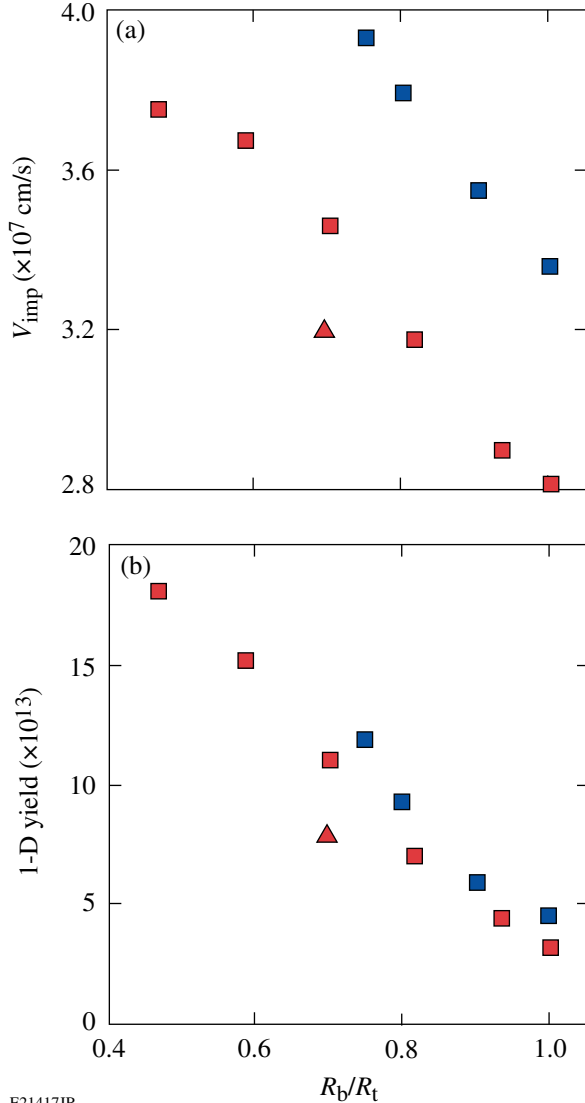
CBET. Figure 133.43 shows that this increased absorption leads to an increased implosion velocity and a factor-of-3 increase in the 1-D predicted neutron yield.

For these simulations (square symbols), the ZPP profiles are given by

$$I_i = P \frac{\exp\left[-\left(r/r_i\right)^{m_i}\right]}{\int \exp\left[-\left(r/r_i\right)^{m_i}\right] r dr},$$

where P is the laser power, i indicates the parameter during the pickets ($i = p$) or main drive ($i = d$), $m_p = 4$, $r_p = 353 \mu\text{m}$ (corresponding to $R_b/R_t = 1$, where R_b is the 95% encircled-energy radius), $m_d = 4$, and r_d was varied from $182 \mu\text{m}$ ($R_b/R_t = 0.5$) to $353 \mu\text{m}$ ($R_b/R_t = 1$).

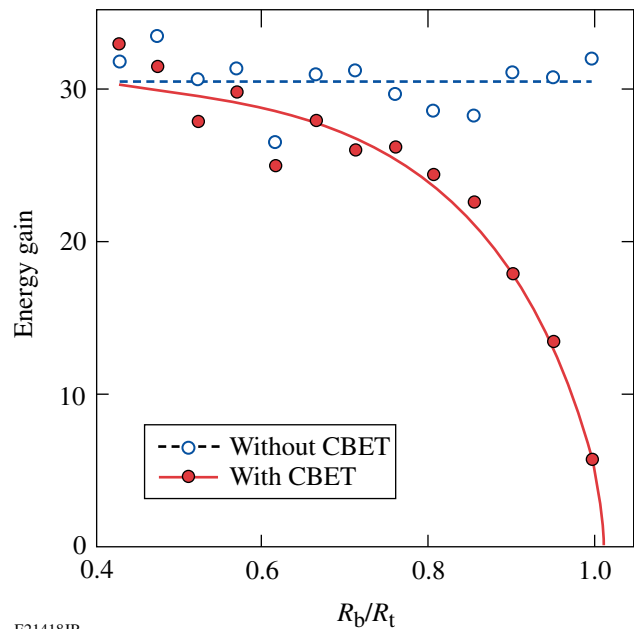
For the 1.5-MJ symmetric direct-drive-ignition design,⁶ zooming can recover a significant portion of the ablation pressure lost to CBET.¹⁹ Figure 133.44 shows that reducing the diameter of the laser beams by 30% is sufficient to recover 90% of the calculated 1-D gain when simulated without including CBET. For a fixed ignition margin ($E_{KE}/E_{\min} \propto \text{IFAR}^3 P_a^3$,



E21417JR

Figure 133.43

The calculated (a) implosion velocity and (b) 1-D yield are plotted as functions of the normalized laser-beam radius for the main drive pulse for two typical low-adiabat OMEGA cryogenic conditions. Low-mass targets ($10 \mu\text{m}$ of CD + $44\text{-}\mu\text{m}$ -thick DT shells) (blue) and higher-mass targets ($9.5 \mu\text{m}$ of CD + $66\text{-}\mu\text{m}$ -thick DT shells) (red) corresponding to OMEGA shots 66612 and 55722, respectively, with optimal zooming profiles (squares) are shown. The predictions using the proposed OMEGA zooming scheme (triangles) are shown. The total energy on target was $\sim 25 \text{ kJ}$, corresponding to an overlap intensity $I_{\text{ovr}} = 8.8 \times 10^{14} \text{ W/cm}^2$.



E21418JR

Figure 133.44

The 1-D gain is calculated for a series of symmetric simulations where the ratio of the laser-beam radius to the target radius ($R_t = 1.7 \text{ mm}$) is varied. The design parameters are taken from Ref. 6.

where IFAR is a measure of the target stability), this increased ablation pressure increases the stability of the implosions ($\text{IFAR} \propto 1/P_a$), providing a more-robust design.

Implications of Zooming on Direct-Drive Implosions

The following section presents the proposed zooming scheme, defines the zooming laser-spot profiles (consistent with OMEGA capabilities), and addresses both the hydrodynamic efficiency (1-D physics) and the hydrodynamic stability (2-D physics) of the OMEGA cryogenic direct-drive target design. Specifically, the hydrodynamic efficiency is increased by the reduced diameter of the laser beams (i.e., reduced CBET) and the increased energy in the normal rays (i.e., energy deposition closer to the ablation surface). The hydrodynamic efficiency may be reduced if the increased single-beam laser intensity exceeds the backscatter thresholds. The hydrodynamic stability is potentially affected by the reduced diameter of the laser beams during the main drive (low mode) and the reduced power spectrum during the pickets (high-frequency imprint).

1. Proposed Focal-Zooming Scheme

a. Time-dependent near field. The basic construct for the time-dependent near-field profile involves a sub-aperture beam for the initial pickets with a full-size beam for the main pulse. The area of each beam depends on three considerations: beam intensity to prevent laser damage, controlled power spectrum to obtain irradiation uniformity, and the stored energy in the beamline.

Based on the maximum required picket power (~ 0.12 TW/beam) and the currently allowed intensity, the minimum sub-aperture beam diameter during the pickets is 14 cm. This sub-aperture beam is half of the nominal diameter and would limit the total energy on target to 75% of the maximum OMEGA energy if an annular main drive pulse were used. The proposed OMEGA zooming scheme will implement a full-aperture beam during the main drive [Fig. 133.40(b)].

b. Zooming phase plates. The proposed zooming approach is made possible by designing a ZPP containing a central region that produces a larger focal spot, while its outer annular region produces a smaller, high-order focal spot. During the picket pulses, a small-diameter beam propagates through the center region of the ZPP, producing a large focal spot. This configuration produces a small central focal spot on top of a lower-intensity larger profile defined by the center of the ZPP. The design methodology for this ZPP involves using a deeper surface relief in the central region, with a smaller one in the annular region of the phase plate. A slowly varying, continu-

ous surface relief is required to reduce the near-field irradiance modulation imposed on the optics at the end of the laser.

The laser profiles consistent with the OMEGA capabilities (“OMEGA ZPP”) are shown in Fig. 133.45. The laser profiles during the pickets are defined by the central 14-cm diameter of the ZPP. Their intensity profiles are given by

$$I_p = P \frac{\exp\left[-\left(r/r_p\right)^{m_p}\right]}{\int \exp\left[-\left(r/r_p\right)^{m_p}\right] r dr},$$

where $m_p = 4$ and $r_p = 365 \mu\text{m}$ (corresponding to a 95% encircled energy radius $R_b = 430 \mu\text{m}$).

After the third picket, the OMEGA beams will use the full aperture (28-cm diameter). The outer ring of the ZPP will produce a high-order super-Gaussian profile. The profile during the drive will consist of the sum of the two profiles, where 3/4 of the total laser power will be within the higher-order profile and 1/4 in the lower-order profile,

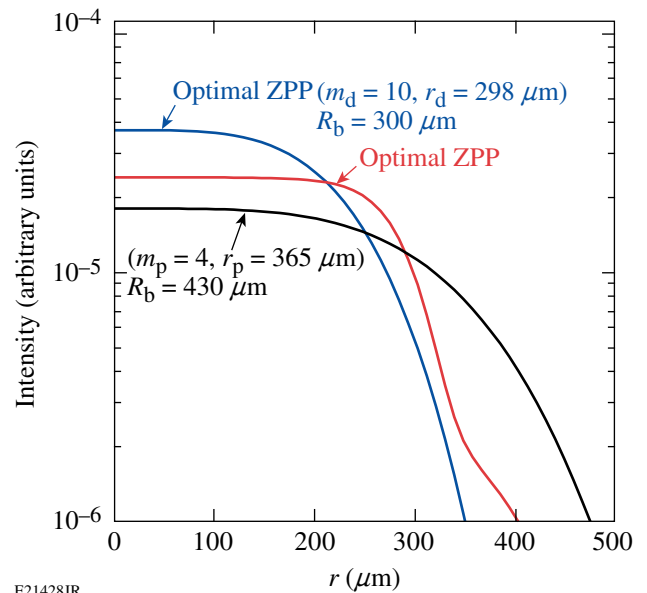


Figure 133.45

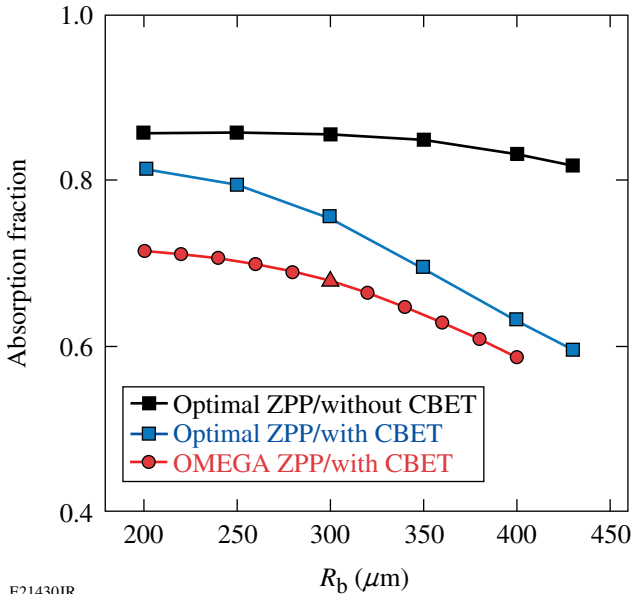
The proposed OMEGA ZPP profiles of the laser beams during the pickets (black curve) and during the main drive (red curve). The more-optimal ZPP profile $R_b/R_t = 0.7$ (blue curve) is shown for $R_b = 300 \mu\text{m}$. The profiles are normalized to the laser power.

$$I_d = P \left\{ \frac{1}{4} \frac{\exp[-(r/r_p)^{m_p}]}{\int \exp[-(r/r_p)^{m_p}] r dr} + \frac{3}{4} \frac{\exp[-(r/r_d)^{m_d}]}{\int \exp[-(r/r_d)^{m_d}] r dr} \right\},$$

where $m_d = 10$ and $r_d = 298 \mu\text{m}$ (corresponding to a 95% encircled energy radius of $R_b = 300 \mu\text{m}$). The lower-order profile is determined by the picket profile but is slightly modified as a result of turning SSD off (not included in this analysis). With the current rectangular SSD kernel ($1.5 \text{ \AA} \times 3.0 \text{ \AA}$), the laser spots during the drive will be slightly elliptical unless compensated for by the ZPP. The ZPP's will be designed to account for the slight ellipticity introduced by the distributed polarization rotators (see Appendix A.1).

2. Hydrodynamic Efficiency (1-D Physics)

a. Cross-beam energy transfer. Figure 133.46 shows results from hydrodynamic simulations with (blue squares) and without CBET (black squares). For the nominal laser beam radii ($R_b/R_t = 1$), CBET reduces the absorption from 82% to 60%. Using the more-optimal ZPP profiles and reducing their radii to $R_b = 300 \mu\text{m}$ ($R_b/R_t = 0.7$), the system recovers more than



E21430JR

Figure 133.46

A comparison of the absorption calculated when including CBET for the zooming configurations with the more-optimal ZPP (squares) and the OMEGA ZPP scheme (circles). The proposed OMEGA zooming profile is shown (triangle). For comparison, simulations without CBET using the more-optimal ZPP scheme are shown (black squares). The overlapped intensity is $8 \times 10^{14} \text{ W/cm}^2$ in all simulations. Shot parameters correspond to OMEGA shot 55722.

70% of the absorbed energy lost to CBET. This is compared with hydrodynamic simulations that use the proposed OMEGA ZPP profiles. For the OMEGA ZPP profile (triangle), CBET is reduced and recovers 35% of the absorbed energy lost to CBET. The residual wings in the laser-beam profiles during the drive (Fig. 133.45) limit the ability of zooming to completely mitigate CBET. The OMEGA ZPP configuration increases the velocity of the thick-target design ($9.5 \mu\text{m}$ of CD + $66 \mu\text{m}$ of DT) from $2.8 \times 10^7 \text{ cm/s}$ ($R_b/R_t = 1$) to $3.2 \times 10^7 \text{ cm/s}$ and the corresponding 1-D predicted neutron yield increases from 3.4×10^{13} to 7.8×10^{13} (Fig. 133.43). For a less-massive target ($10 \mu\text{m}$ of CD + a $44\text{-}\mu\text{m}$ -thick DT shell), the velocity for $R_b/R_t = 0.7$ is $4.1 \times 10^7 \text{ cm/s}$ when using the more-optimal beam profiles during the drive, compared to an estimated $3.7 \times 10^7 \text{ cm/s}$ when using the OMEGA ZPP profiles.

b. Laser-plasma interactions. Reducing the radii of the beams during the drive increases the single-beam laser intensity. In typical cryogenic designs on OMEGA, where $R_b/R_t = 1$, the peak single-beam intensity is approximately

$$I_p(r=0) \cong \frac{8}{N} I_{\text{ovr}} \sim 1.2 \times 10^{14} \text{ W/cm}^2,$$

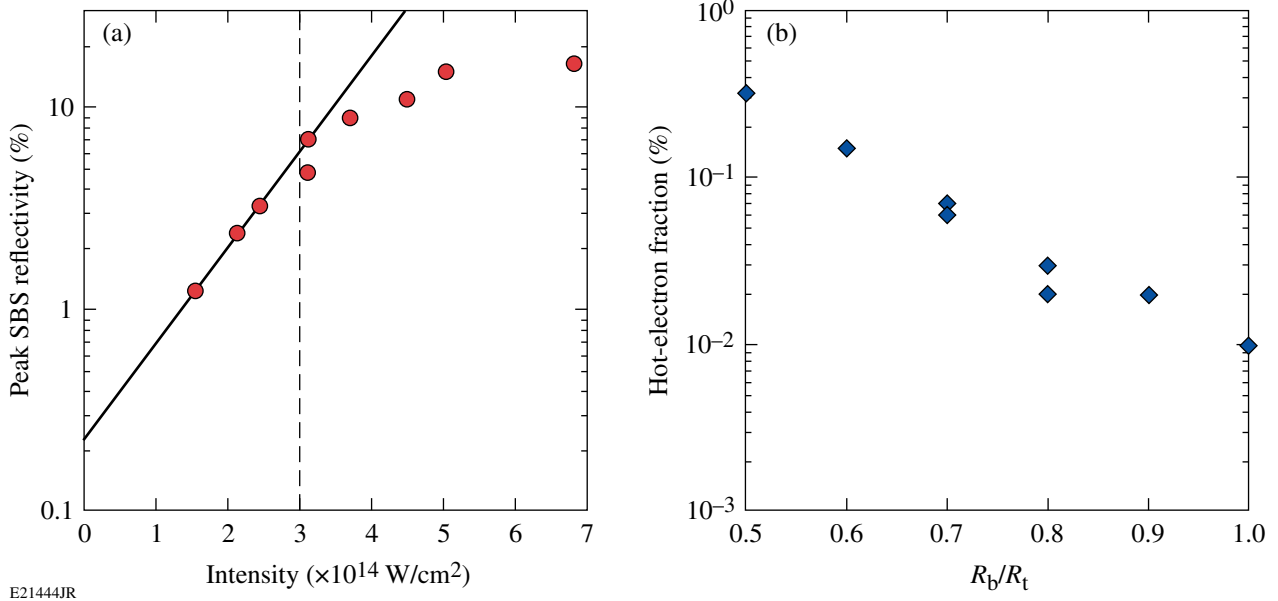
where $N = 60$ is the number of beams, $I_{\text{ovr}} = P_d/A_t = 8.8 \times 10^{14} \text{ W/cm}^2$, $P_d = 20 \text{ TW}$ is the power in the drive, and A_t is the surface area of the target. The single-beam intensity is increased as the radii of the beams are reduced:

$$I_d(r=0) \cong 1.2 \times 10^{14} \left(\frac{R_t}{R_b} \right)^2 \text{ W/cm}^2.$$

For $R_b = 300 \mu\text{m}$, the corresponding single-beam intensity during the drive is $\sim 2.5 \times 10^{14} \text{ W/cm}^2$.

Figure 133.47(a) shows the measured peak SBS reflectivity threshold for OMEGA direct-drive plasmas. Exceeding the SBS intensity thresholds will backscatter laser light from the target, reducing the drive efficiency. These results suggest that the peak laser intensities must remain below $3 \times 10^{14} \text{ W/cm}^2$ to keep SBS from becoming energetically significant, but this threshold depends on the exact plasma conditions.

Experiments on OMEGA show an increase in the hot-electron fraction when reducing the radii of the laser beams (see Ref. 18 for the experimental setup). Figure 133.47(b) shows that the fraction of laser energy converted to hot electrons increased by more than an order of magnitude when the radii of the laser beams were changed from $430 \mu\text{m}$ to $215 \mu\text{m}$.



E21444JR

Figure 133.47

(a) The peak SBS reflectivity measured from OMEGA 860- μ m-diam CH implosion experiments is shown as a function of the peak single-beam laser intensity. The SBS reflectivity peaks during the intensity rise in the main drive pulse when the electron temperature is low. (b) The fraction of laser energy converted to hot electrons inferred from hard x-ray measurements is shown as a function of the radii of the laser beams normalized to the target radius ($R_t = 430 \mu\text{m}$). The overlapped intensity was held nearly constant at 4.5×10^{14} W/cm².

3. Hydrodynamic Stability (2-D Physics)

a. Low-mode stability. Two-dimensional *DRACO*²⁷ simulations were performed to investigate the level of perturbations induced by the lower illumination uniformity when the diameter of the laser beams were reduced at various times in the laser pulse. The simulations use a cryogenic, low-adiabat, triple-picket implosion design (OMEGA shot 55722, 9.5 μm of CD + a 66- μm -thick DT shell). The simulations that do not include CBET employ a thermal-transport model where the heat flux was limited to a fraction ($f = 0.06$) of the free-streaming flux.²⁸ This is a reasonable approach since 1-D simulations indicate very little effect from CBET for these conditions (i.e., $R_b/R_t = 0.7$).

Figure 133.48 shows simulated shell densities at maximum compression. Improvements in target uniformity are clearly seen in Fig. 133.48(b), where two-state zooming was applied after the third picket in comparison with those simulations where zooming was not used [Fig. 133.48(a)]. Table 133.VII summarizes the performance of simulated targets depending on the transition time from large- to small-diameter beams. At peak neutron flux, the normalized areal-density perturbations (Σ_{rms}) are shown and quantify the effect of the overlapped nonuniformities. These results indicate that the amplitude of perturbations is reduced by an order of magnitude when the

Table 133.VII: A summary of the effect of zooming on areal-density perturbations at peak neutron flux when zooming at different times from $R_b/R_t = 1.0$ to $R_b/R_t = 0.7$.

Zooming	R_b/R_t	Σ_{rms} (%)
Not applied	0.7	9
After first picket	1.0 to 0.7	7
After second picket	1.0 to 0.7	1.1
After third picket	1.0 to 0.7	1.1
At beginning of main pulse	1.0 to 0.7	1.1
Not applied	1.0	1.2

transition occurs after the second or third picket and that zooming between the third picket and the main pulse will maintain target uniformity while mitigating CBET.

b. High-frequency imprint. The proposed OMEGA zooming scheme requires that the near-field diameter be reduced by a factor of 2 to produce larger laser spots during the pickets. This reduced near-field diameter may impact the target performance by increasing the rms (root-mean-square) illumination nonuniformity. Figure 133.49 shows the ratio of the ℓ -mode σ_{rms} amplitude spectrum for the OMEGA ZPP design during the pickets ($D_{\text{ZPP}} = 14$ cm) to the standard OMEGA configuration ($D = 28$ cm). The ℓ -mode σ_{rms} is given by²⁹

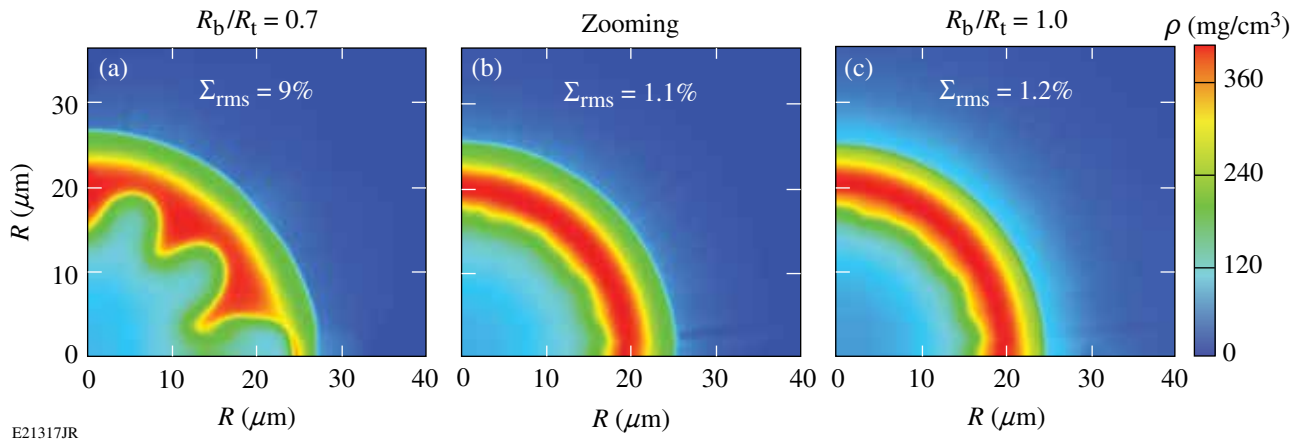


Figure 133.48

Simulated shell density at maximum compression in the case of using (a) small-diameter beams ($R_b/R_t = 0.7$) for the entire laser pulse, (b) large-diameter beams ($R_b/R_t = 1$) for pickets and small-diameter beams ($R_b/R_t = 0.7$) for the main pulse, and (c) large-diameter beams for the entire pulse.

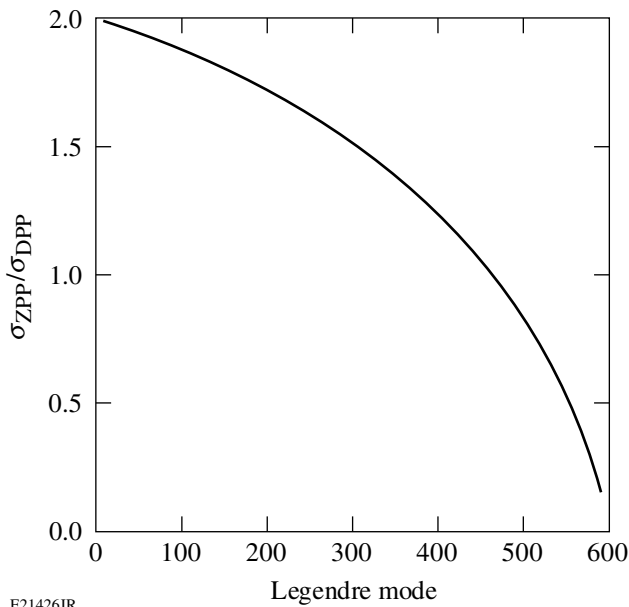


Figure 133.49

The ratio of rms (root-mean-square) illumination uniformity for the sub-aperture pickets (half-aperture) over the standard OMEGA full-aperture configuration is plotted against the Legendre mode for a target radius of 430 μm .

$$\sigma_l^2 = \frac{16}{\pi \ell_{\max}} \frac{\ell}{\ell_{\max}} \times \left[\cos^{-1} \left(\frac{\ell}{\ell_{\max}} \right) - \left(\frac{\ell}{\ell_{\max}} \right) \sqrt{1 - \left(\frac{\ell}{\ell_{\max}} \right)^2} \right],$$

where $\ell_{\max} = Rk_{\max} = 2\pi R/F\#\lambda$, $R = 460 \mu\text{m}$ is the target radius, $F\# = FL/D$, $FL = 190 \text{ cm}$, and D is the diameter of the beam at the lens plane.

Over the range of modes that most significantly impacts target performance (10 to 300), σ_{rms} increases by a factor of nearly 2. In addition, the $4\times$ reduction in beam area will result in fewer speckles to fill out the envelope and the focal spot will contain a lumpy pattern. An assessment of the impact of increased illumination uniformities will be performed but mitigation strategies have been demonstrated that reduce imprint by a factor of 2 when using doped ablaters.^{22,23} Although a larger beam size during the pickets would fill out the power spectrum, the correspondingly larger central region of the ZPP would increase the energy in the tails of the beam profiles during the drive and would increase CBET.

Propagation of a beam with a half diameter through the current SSD system will produce 1.5 color cycles over the beam rather than the current three color cycles. Although the angular dispersion remains constant, the simultaneity of the colors in the spectrum is not guaranteed and a certain amount of modulation frequency may appear in the integrated focal spot on target, i.e., unwanted pulse shaping. If this is found to be a problem for the experiment, the SSD system will need to be modified.

4. Target Physics Requirements for Zooming on OMEGA

The physics requirements for zooming are based on demonstrating implosion performance on OMEGA that is hydrodynamically equivalent to a 1.5-MJ ignition implosion on the National Ignition Facility (NIF). This requires a Lawson criteria³⁰ $\left[\chi \approx (\rho R)^{0.6} (0.24 Y_n / M_{\text{fuel}})^{0.3} \right]$ of $\chi = 0.16$, where ρR is in g/cm^2 , Y_n is the yield in units of 10^{16} , and M_{fuel} is the mass of the fuel in milligrams (mg) (Ref. 31). For the total laser energy available on OMEGA, this corresponds to a ρR of

300 mg/cm² and a yield of 4×10^{13} . Currently, the best implosions on OMEGA produce a yield of 2.1×10^{13} and a ρR of 160 mg/cm² corresponding to $\chi = 0.09$ (Ref. 32). Mitigation of CBET will increase the ablation pressure, providing both a higher ρR ($\rho R \propto \sqrt{P_a}$) and a higher yield ($Y \propto P_a$). The physics requirements for zooming on OMEGA are based on increasing the ablation pressure by reducing CBET without imposing deleterious effects through nonuniformities or laser–plasma interactions. The following section provides the physics basis for the OMEGA zooming design and presents the main logic used to determine the requirements summarized in Table 133.VIII.

Table 133.VIII: Target physics requirements for zooming on OMEGA.

	R_b (μm)	Power spectrum	SG order	Peak power (TW/beam)
Pickets	430	See below*	4	0.12
Drive	365**	Best effort	2 to 20	0.35

*See **Power Spectrum (Pickets)** below.

See **Drive-Beam Radius below.

a. Picket-beam radius. The radii of the laser beams during the pickets are defined to maximize illumination uniformity and minimize the energy lost outside of the target. The proposed design assumes that the current SG4 distributed phase plate (DPP) profiles are optimized ($m = 4$, $r = 365 \mu\text{m}$). A further optimization study could be performed to characterize the effect of reducing the picket-beam radius on the illumination nonuniformities and the CBET during the drive; reducing the beam radius during the pickets will reduce the wings in the drive profile.

b. Drive-beam radius. The minimum drive-beam radius is governed by the acceptable low-frequency modulations and the acceptable laser–plasma interaction intensity thresholds. The maximum drive-beam radius is governed by the required reduction in CBET to regain hydrodynamically equivalent implosions on OMEGA. A minimum radius of $R_b = 300 \mu\text{m}$ is proposed to ensure that the peak intensity remains below the intensity, where SBS scatters <5% of the incident laser light.

c. Power spectrum (pickets). The power spectrum between Legendre modes 10 and 300 has the largest impact on target performance. A study will be performed to assess the impact of the increased power spectrum over these modes, but mitigation strategies exist that can reduce the imprint by a factor of 2 (Refs. 22 and 23).

d. Super-Gaussian order (pickets). To maintain reasonable illumination uniformities during the pickets, a super-Gaussian order consistent with the current OMEGA SG4 design ($m = 4$) is proposed.^{33,34} With the OMEGA near-field limitations during the drive, increasing the super-Gaussian order may reduce CBET; a further study will be performed to optimize this gain with the loss of illumination uniformity.

e. Super-Gaussian order (drive). A series of 1-D LILAC simulations were performed to investigate the sensitivity of CBET to the super-Gaussian order of the laser beams during the main drive. In these simulations the profile of the laser beams during the pickets was given by a fourth-order super-Gaussian with 95% of the energy contained within the target diameter ($2R_t = 860 \mu\text{m}$), and the super-Gaussian order during the main drive was varied between 2 and 20 [Fig. 133.50(a)] while maintaining 95% of the energy within $R_b = 300 \mu\text{m}$. Figure 133.50(b) shows a small effect on the laser-beam absorption. For a given laser power and spot size, high-order super-Gaussian beam profiles reduce the peak intensities limiting the risk of laser–plasma instabilities.

f. Peak power (pickets). The picket-pulse shapes (timing and peak powers) are used to set the adiabat, and it is not currently envisioned that the peak power in the pickets will exceed 0.12 TW. This peak power must be consistent with the diameter of the laser beams during the pickets to ensure the laser system remains below damage thresholds.

g. Peak power (drive). The current cryogenic target design uses 25 kJ of energy to produce a peak power of nearly 0.35 TW in the drive.

5. Proposed Physics Studies

Several physics issues are identified that require further study:

1. The fraction of laser energy converted to hot electrons will be measured and their impact on target performance assessed for laser beams with $R_b = 300 \mu\text{m}$, producing an overlapped intensity of $8 \times 10^{14} \text{ W/cm}^2$ on a standard 430- μm -radius target.
2. The impact of the increased power spectrum during the pickets on the OMEGA implosion performance will be studied and mitigation strategies developed to reduce the effects of imprint.
3. A study is required to optimize the picket-beam profiles. Because the drive pulse shares the central portion of the ZPP with the pickets, the picket profile defines the wings during the main pulse. Reducing the beam radius or increasing the super-Gaussian order during the pickets will further reduce CBET but may increase laser imprint.

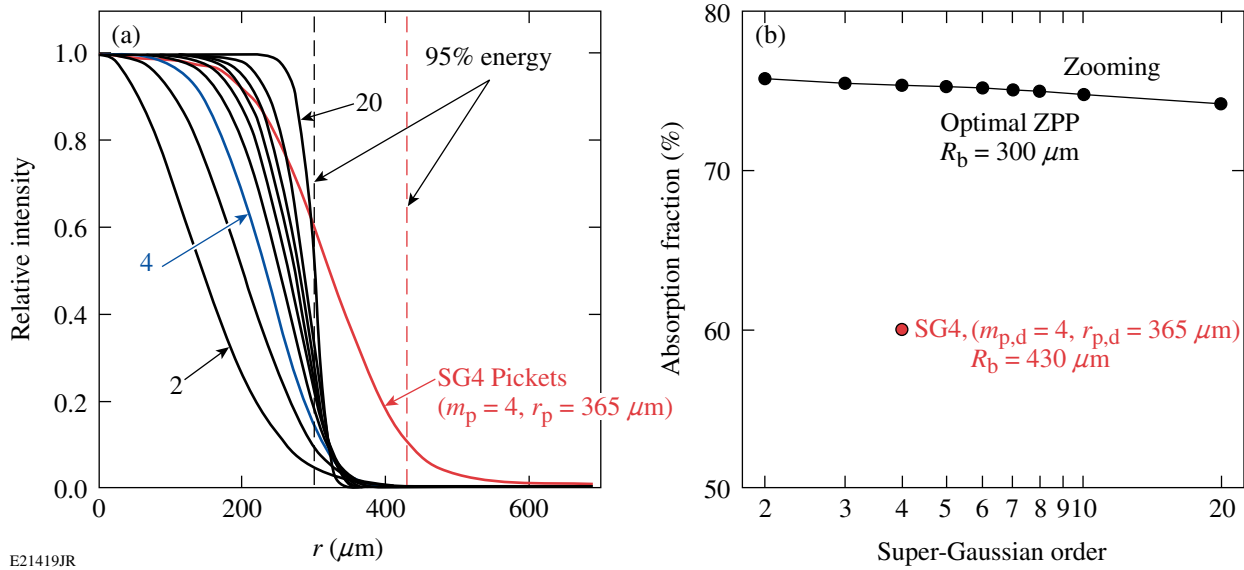


Figure 133.50

The profiles used in simulations to investigate the sensitivity of CBET to super-Gaussian order during the main drive. (a) The profiles in the main drive were varied by changing the super-Gaussian order between 2 and 20 while maintaining 95% of the energy within $R_b = 300 \mu\text{m}$. (b) The effect of super-Gaussian order over this range has a small effect on total absorption.

- The $4\times$ reduction in the area of the laser beam during the pickets will result in fewer speckles to fill out the envelope and the focal spot could contain lumps. This effect on target performance will be assessed by simulating the implosion performance using the calculated ZPP phase.

Implementation of Zooming on OMEGA

The proposed implementation of zooming on OMEGA requires a dynamic two-state near-field profile and a set of ZPP's. To generate the required two-state near-field profile, a dual-driver co-propagation configuration is proposed. The driver that will generate the pickets will contain the current rectangular SSD kernel and pass through an apodizer, forming a beam of half the standard diameter. A second driver will generate the drive pulse and propagate without SSD through its own apodizer, forming a full-diameter beam.

Implementation of focal-spot zooming on OMEGA will require the development of a new main-pulse driver (zooming driver) that can be combined and co-propagated with the current SSD driver after the SSD modulators (Fig. 133.51). By combining the drivers at the base of the periscope, the losses introduced by the combining optic can be offset by rebalancing the engineered losses that currently exist at the output of the regenerative amplifier. The driver combination would be located before the G4 grating(s). To compensate for the G4

grating(s), a G3 surrogate grating would be integrated into the zooming driver line to apply the required spatiotemporal shear to precompensate for the G4 grating.

An initial study of implementing zooming on OMEGA indicates no technical limitations. Introducing a dual-driver co-propagation configuration will provide (1) a 14-cm-diam beam during the pickets ($1.5\text{-}\text{\AA} \times 3\text{-}\text{\AA}$ SSD) and a full-aperture, 28-cm-diam beam (no SSD) during the main drive; and (2) an $\sim 10\%$ increase in on-target energy as a result of better frequency-conversion efficiency.

Summary

To demonstrate hydrodynamic-equivalent ignition performance on OMEGA, CBET must be mitigated. For a nominal direct-drive configuration, CBET scatters $\sim 20\%$ of the laser energy from the target, reducing the ablation pressure by 40%. This reduced ablation pressure impacts the direct-drive implosions by reducing the hot-spot pressure and the implosion velocity. This results in a lower yield and reduced stability of the implosion when maintaining a constant minimum energy. On OMEGA cryogenic implosions, the reduced ablation pressure results in an order-of-magnitude reduction in yield. Reducing the radii of the laser beams during the main drive, while maintaining the nominal radius of the laser beams during the pickets (two-state zooming),¹⁹ is shown to significantly reduce

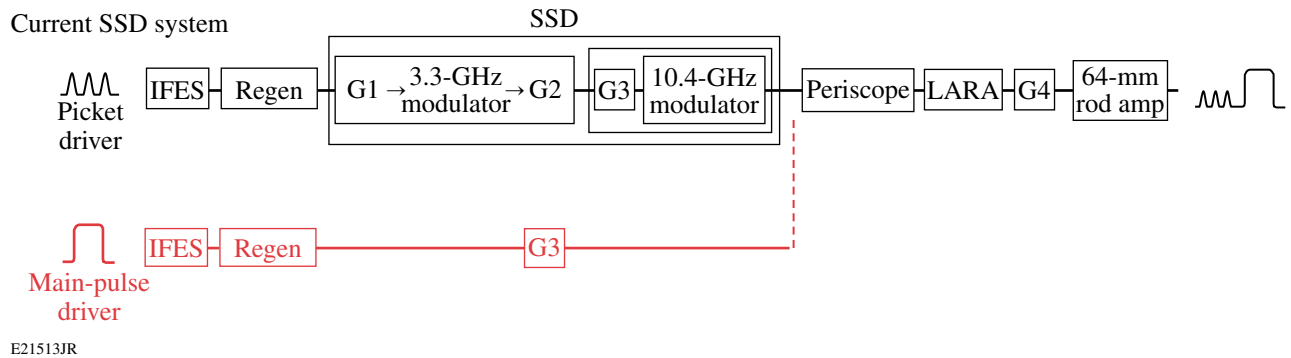


Figure 133.51

The current smoothing by spectral dispersion (SSD) driver line (black) and the proposed zooming drive line (red) are shown. IFES: integrated front-end source; Regen: regenerative amplifier; LARA: large-aperture ring amplifier.

CBET while maintaining high-quality implosions. A two-state zooming scheme is proposed for OMEGA that will recover 35% of the energy lost to CBET.

Implementing zooming on OMEGA will require a new set of phase plates and a dynamic near-field profile. The proposed dynamic near-field profile can be produced using a co-propagating dual-driver configuration. The initial driver line would produce the pickets and propagate through the central half-diameter of the laser system, while the second driver would produce the drive pulse and propagate through the full aperture of the laser system. The central 14-cm diameter of the radially varying phase plates would produce the nominal laser profile on target during the pickets and a smaller radius profile during the main drive.

Implementing zooming on OMEGA will provide a higher hydrodynamic efficiency that will allow targets to be driven faster with higher stability and is equivalent to an increased velocity corresponding to a 30% increase in the on-target laser energy.

ACKNOWLEDGMENT

This work was supported by the U.S. Department of Energy Office of Inertial Confinement Fusion under Cooperative Agreement No. DE-FC52-08NA28302, the University of Rochester, and the New York State Energy Research and Development Authority. The support of DOE does not constitute an endorsement by DOE of the views expressed in this article.

Appendix A: Alternate Concepts for Zooming on OMEGA

Additional focal-zooming schemes are available for consideration. The zooming effect from 2-D SSD is proportional to the bandwidth, the grating dispersion, and the focal length of the final lens. Increasing either the bandwidth or the grating dispersion on OMEGA would necessarily require opening

the spatial-filter apertures. Placing the final dispersion grating closer to the end of each beamline would allow greater angular dispersion without the risk of damaging the laser chain. Alternatively, the focal length of the final lens could be increased to achieve larger deflection at the focal plane. In this case the focal lens assemblies would be positioned within the hex tubes and the vacuum windows would be repositioned outside the surface of the target chamber rather than being re-entrant. Another option involves using a circular grating at the end of the system to provide both beam smoothing and focal-plane broadening.

1. Zooming with Enhanced 2-D SSD Reduction

An alternative approach to zooming that takes advantage of the reduced deflection that occurs when SSD is turned off was investigated. This approach could achieve the optimum reduction of CBET (i.e., no wings in the profiles during the main drive) but requires that the SSD deflection be symmetric and significantly increased to achieve a change in the focal-spot radius of $65 \mu\text{m}$ (from $430 \mu\text{m}$ to $365 \mu\text{m}$ for equivalent ZPP scheme performance). This initial study indicates that the small SSD dimension could be doubled to form a symmetric 2-D SSD kernel that would produce an $\sim 35\text{-}\mu\text{m}$ change in the focal-spot radius, but it is unlikely that a further increase to accommodate the required deflection is feasible.

Currently, laser-beam smoothing on the OMEGA 60-beam system includes 2-D SSD and distributed polarization rotation (DPR). The 2-D angular deflection kernel is square and consists of SSD deflection in the first dimension with a 50/50 combination of SSD and DPR deflections in the second dimension. The magnitude of angular deflection from SSD is the product of the angular dispersion and the bandwidth. The angular deflection from the DPR is set by the wedge in the birefringent plate. The

resulting spatial shift in the focal plane is the product of the total angular deflection and the focal length of the lens.

To fully benefit from SSD broadening in two dimensions, the wedged DPR is removed, while the second dimension of SSD is doubled in magnitude. This could be achieved by either doubling the bandwidth or doubling the angular dispersion, or an optimized combination of both. The resulting focal spots would be nominally round either with or without 2-D SSD. Downward zooming would be achieved by turning off the bandwidth, and, therefore, the deflection kernel, in such a way that a smaller monochromatic focal spot would irradiate the target. In this scenario, a 2-D symmetric SSD kernel would be turned off after the pickets and before the main pulse.

a. Ability for OMEGA to support a symmetric 2-D SSD kernel. Removing the current DPR's and making the resultant rectangular far-field kernel square by increasing the deflection Γ in the narrow dimension were investigated to determine if a symmetric SSD kernel could be supported by the OMEGA system. Since the far-field deflection is the product of the frequency dispersion ($\partial\theta/\partial\lambda$) and the total bandwidth $\Delta\lambda$, the deflection may be increased by increasing either the dispersion or the total bandwidth.

Prior to addressing changes to OMEGA that are required to support the symmetric kernel, the current state of SSD on OMEGA was assessed. The current implementation of three-color-cycle SSD consists of 1.5 Å of FM bandwidth at 3.3 GHz dispersed in the phase-matching direction of the frequency doubler and 3.0 Å of FM bandwidth at 10.4 GHz dispersed in the phase-matching direction of the tripler. The dispersion, measured at the 30-cm output aperture of OMEGA, is $32 \mu\text{rad}/\text{Å}$ in both directions. In the absence of any aberrations, this results in a rectangular far field with a 2:1 aspect ratio [Fig. 133.52(a)]. The actual far-field pattern is a convolution of the theoretical rectangle with the aberrated, undispersed focal spot.

Figure 133.52(b) shows an estimated OMEGA IR far-field spot along with the limiting pinhole aperture in the OMEGA Laser System. Plasma blowoff from laser intensity on the pinhole edges ultimately limits how much dispersed bandwidth can be propagated through OMEGA. This is a statistical function of the deflection, temporal pulse shape, beamline aberration, pulse length, alignment tolerances, and pinhole geometry and cleanliness.

To assess OMEGA's ability to support a symmetric SSD kernel, the required system changes, implications for the

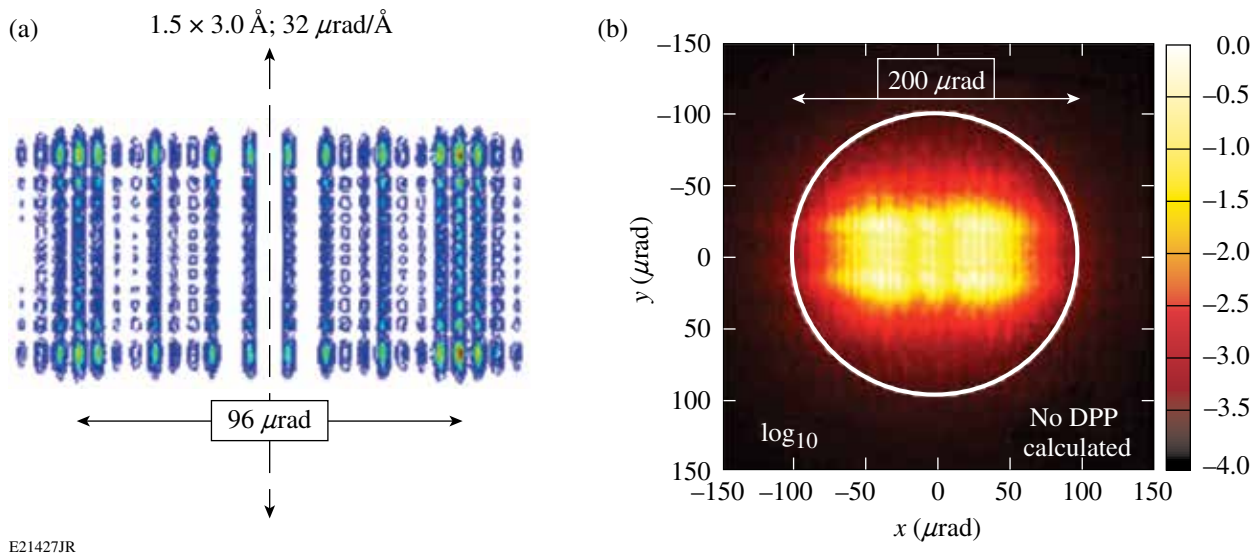


Figure 133.52

(a) The theoretically perfect rectangular far-field pattern. Note the Bessel-function structure in either direction. The narrow (vertical in figure) dimension is the 1.5-Å bandwidth, 3.3-GHz direction; the wide (horizontal in figure) dimension is the 3.0-Å bandwidth, 10.4-GHz direction. (b) Simulated IR \log_{10} far-field spot ($4\times$ diffraction limit) at the 30-cm aperture. The white circle is the aperture of the limiting pinhole calculated at the end of the laser system.

OMEGA pinholes as a result of the focal-spot shape change, and the impact on the frequency-conversion efficiency and potential FM-to-AM effects of the increase in bandwidth and/or dispersion are investigated.

System changes: Achieving a symmetric focal spot requires increasing the far-field deflection of the 3.3-GHz axis. This can be achieved by increasing the bandwidth at 3.3 GHz or increasing the dispersion. Further increases in bandwidth would require testing of the 3.3-GHz modulator, which is currently near its power limit. It is possible that some increase in bandwidth can be realized, but this remains to be experimentally demonstrated. Increasing the dispersion in the 3.3-GHz direction requires that a single grating in the pulse-generation room be replaced with a new grating. The actual implementation of a new grating geometry would require substantial realignment of the 3.3-GHz SSD arm.

Pinhole implications: In the early days of three-color-cycle SSD on OMEGA, it became clear that the current pinhole configuration cannot tolerate any increase in the far-field deflection in the 10.4-GHz direction (wide direction). Any increase in the current OMEGA pinhole size is prohibited by the observed damage rate to the Stage-D, -E, and -F input spatial-filter lenses and the necessity of preventing catastrophic retroreflections in the beamlines. It is possible that the current pinholes could tolerate an increase in the far-field deflection in the narrow 3.3-GHz direction.

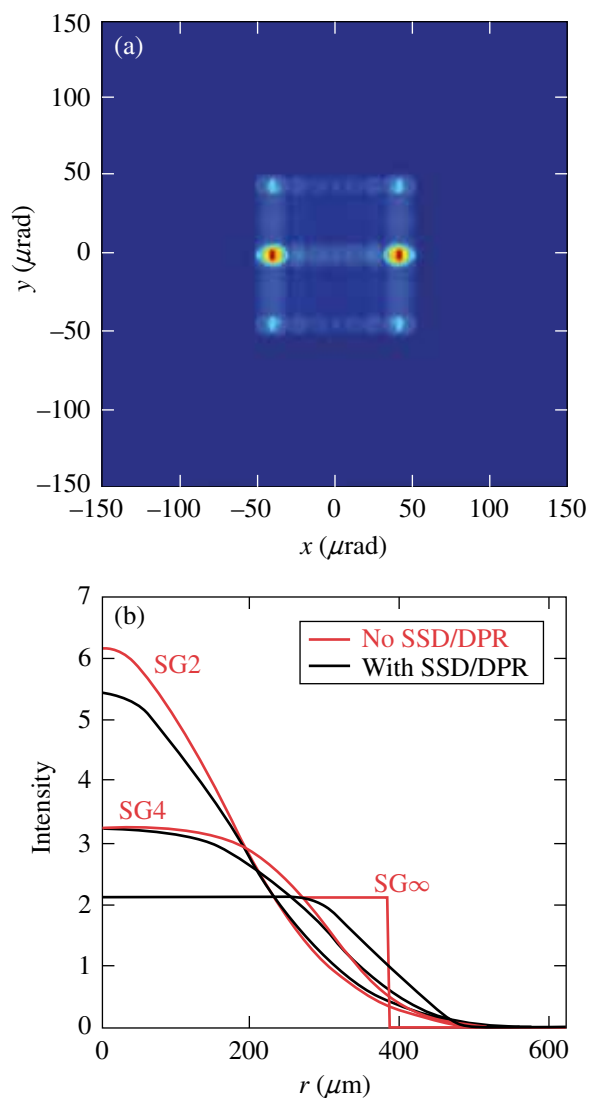
Several factors contribute to the position and size of the focal spot relative to the pinhole. These factors are statistical in nature, so while theoretical calculations can provide an estimate of the amount of deflection in the narrow direction that can be realized, the actual capability of OMEGA to support this change can be measured only via a series of laser shots. This experimental investigation will require a dedicated laser campaign that increases relative deflection while monitoring the transmitted near-field profile, transmitted temporal pulse shape, retroreflected energy, and pinhole-scattered light.

Frequency conversion: A deflection increase in the narrow 3.3-GHz direction has the potential to limit conversion efficiency and introduce FM-to-AM conversion because of the poor conversion efficiency of certain components of the FM spectrum. This loss of frequency conversion can occur regardless of which technique (increased dispersion or increased bandwidth) is used to increase deflection. Both options have been examined with respect to frequency-conversion implica-

tions using the code Miró,³⁵ and preliminary results indicate no preferred method from this standpoint. Implementation difficulty will most probably dictate the choice of technique.

b. Effects of the current OMEGA kernel on the focal spot.

To estimate the effect of 2-D dynamic bandwidth reduction, the best understanding of the current OMEGA SSD/DPR deflection kernel [Fig. 133.53(a)] was used. Figure 133.53(b) shows



E21421JR

Figure 133.53
 (a) The current OMEGA far-field SSD/DPR convolution kernel applied to a diffraction-limited ($\sim 12 \mu\text{m}$ at the target plane) beam (smoothed for presentation purposes). (b) The beam profiles when the current SSD/DPR kernel is applied (black) to the “no SSD/DPR” (red) profiles generated with super-Gaussian orders of 2, 4, and infinity. All beams have a “with SSD/DPR” diameter of $860 \mu\text{m}$.

the effect of this kernel on various laser-beam far-field profiles. Table 133.IX summarizes these results with respect to zooming; the maximum effect occurs for an infinitely steep profile where the 95% encircled-energy radius is increased from 377 μm to 430 μm . To achieve the proposed zooming conditions (430 μm to 300 μm), where 70% of the energy lost to CBET is recovered, the kernel would need to be increased by more than a factor of 2.5. This approach requires that the spatial-filter apertures on OMEGA be increased in size beyond the point considered appropriate for a noisy and aging laser system.

Table 133.IX: The 95% encircled-energy radius increase as a result of SSD/DPR versus order of super-Gaussian of “no SSD/DPR” beam. All beams have a “with SSD/DPR” diameter of 860 μm .

Super-Gaussian order	R_b increase (μm)
2	24.5
4	31.8
6	36.1
8	39.6
10	42.1
20	47.3
100	51.6
∞	52.9

2. New DPR Options

To maintain a round focal spot throughout the laser pulse when implementing zooming with a symmetric 2-D SSD kernel, the wedged DPR’s must be removed from the current system. Polarization smoothing, using advanced DPR’s, could be maintained on OMEGA even with fully dispersive 2-D SSD. Several non-wedged DPR options are being developed for use in polar-drive experiments on the NIF. A 4 \times 4 checkerboard array of left-handed and right-handed glancing-angle deposition coatings are being developed at LLE to provide an improved power spectrum with smoothing. Alternatively, a 2 \times 2 checkerboard array of KD*P half-wave plates and air is the baseline DPR for polar drive on the NIF.

REFERENCES

1. J. Nuckolls *et al.*, Nature **239**, 139 (1972).
2. E. I. Moses and C. R. Wuest, Fusion Sci. Technol. **47**, 314 (2005).
3. C. Cavaller, Plasma Phys. Control. Fusion **47**, B389 (2005).
4. J. D. Lindl *et al.*, Phys. Plasmas **11**, 339 (2004).

5. R. L. McCrory, D. D. Meyerhofer, R. Betti, R. S. Craxton, J. A. Delettrez, D. H. Edgell, V. Yu. Glebov, V. N. Goncharov, D. R. Harding, D. W. Jacobs-Perkins, J. P. Knauer, F. J. Marshall, P. W. McKenty, P. B. Radha, S. P. Regan, T. C. Sangster, W. Seka, R. W. Short, S. Skupsky, V. A. Smalyuk, J. M. Soures, C. Stoeckl, B. Yaakobi, D. Shvarts, J. A. Frenje, C. K. Li, R. D. Petrasso, and F. H. Séguin, Phys. Plasmas **15**, 055503 (2008).
6. V. N. Goncharov, T. C. Sangster, T. R. Boehly, S. X. Hu, I. V. Igumenshchev, F. J. Marshall, R. L. McCrory, D. D. Meyerhofer, P. B. Radha, W. Seka, S. Skupsky, C. Stoeckl, D. T. Casey, J. A. Frenje, and R. D. Petrasso, Phys. Rev. Lett. **104**, 165001 (2010).
7. R. K. Kirkwood *et al.*, Phys. Rev. Lett. **76**, 2065 (1996).
8. W. Seka, H. A. Baldis, J. Fuchs, S. P. Regan, D. D. Meyerhofer, C. Stoeckl, B. Yaakobi, R. S. Craxton, and R. W. Short, Phys. Rev. Lett. **89**, 175002 (2002).
9. J. Myatt, A. V. Maximov, W. Seka, R. S. Craxton, and R. W. Short, Phys. Plasmas **11**, 3394 (2004).
10. P. Michel *et al.*, Phys. Rev. Lett. **102**, 025004 (2009).
11. I. V. Igumenshchev, W. Seka, D. H. Edgell, D. T. Michel, D. H. Froula, V. N. Goncharov, R. S. Craxton, L. Divol, R. Epstein, R. Follett, J. H. Kelly, T. Z. Kosc, A. V. Maximov, R. L. McCrory, D. D. Meyerhofer, P. Michel, J. F. Myatt, T. C. Sangster, A. Shvydky, S. Skupsky, and C. Stoeckl, Phys. Plasmas **19**, 056314 (2012).
12. P. Michel *et al.*, Phys. Rev. E **83**, 046409 (2011).
13. S. H. Glenzer *et al.*, Science **327**, 1228 (2010).
14. J. D. Moody *et al.*, Nat. Phys. **8**, 344 (2012).
15. T. R. Boehly, D. L. Brown, R. S. Craxton, R. L. Keck, J. P. Knauer, J. H. Kelly, T. J. Kessler, S. A. Kumpan, S. J. Loucks, S. A. Letzring, F. J. Marshall, R. L. McCrory, S. F. B. Morse, W. Seka, J. M. Soures, and C. P. Verdon, Opt. Commun. **133**, 495 (1997).
16. W. Seka, D. H. Edgell, J. P. Knauer, J. F. Myatt, A. V. Maximov, R. W. Short, T. C. Sangster, C. Stoeckl, R. E. Bahr, R. S. Craxton, J. A. Delettrez, V. N. Goncharov, I. V. Igumenshchev, and D. Shvarts, Phys. Plasmas **15**, 056312 (2008).
17. I. V. Igumenshchev, D. H. Edgell, V. N. Goncharov, J. A. Delettrez, A. V. Maximov, J. F. Myatt, W. Seka, A. Shvydky, S. Skupsky, and C. Stoeckl, Phys. Plasmas **17**, 122708 (2010).
18. D. H. Froula, I. V. Igumenshchev, D. T. Michel, D. H. Edgell, R. Follett, V. Yu. Glebov, V. N. Goncharov, J. Kwiatkowski, F. J. Marshall, P. B. Radha, W. Seka, C. Sorce, S. Stagmitto, C. Stoeckl, and T. C. Sangster, Phys. Rev. Lett. **108**, 125003 (2012).
19. I. V. Igumenshchev, D. H. Froula, D. H. Edgell, V. N. Goncharov, T. J. Kessler, F. J. Marshall, R. L. McCrory, P. W. McKenty, D. D. Meyerhofer, D. T. Michel, T. C. Sangster, W. Seka, and S. Skupsky, “Laser-Beam Zooming to Mitigate Crossed-Beam Energy Losses in Direct-Drive Implosions,” to be published in Physical Review Letters.
20. M. C. Myers *et al.*, Nucl. Fusion **44**, S247 (2004).

21. S. Skupsky, R. W. Short, T. Kessler, R. S. Craxton, S. Letzring, and J. M. Soures, *J. Appl. Phys.* **66**, 3456 (1989).
22. G. Fiksel, S. X. Hu, V. N. Goncharov, D. D. Meyerhofer, T. C. Sangster, V. A. Smalyuk, B. Yaakobi, M. J. Bonino, and R. Jungquist, *Phys. Plasmas* **19**, 062704 (2012).
23. S. X. Hu, G. Fiksel, V. N. Goncharov, S. Skupsky, D. D. Meyerhofer, and V. A. Smalyuk, *Phys. Rev. Lett.* **108**, 195003 (2012).
24. M. C. Herrmann, M. Tabak, and J. D. Lindl, *Phys. Plasmas* **8**, 2296 (2001).
25. "Cross-Beam Energy Transfer in Polar-Drive Implosions on OMEGA," published in this volume.
26. J. Delettrez, *Can. J. Phys.* **64**, 932 (1986).
27. P. B. Radha, T. J. B. Collins, J. A. Delettrez, Y. Elbaz, R. Epstein, V. Yu. Glebov, V. N. Goncharov, R. L. Keck, J. P. Knauer, J. A. Marozas, F. J. Marshall, R. L. McCrory, P. W. McKenty, D. D. Meyerhofer, S. P. Regan, T. C. Sangster, W. Seka, D. Shvarts, S. Skupsky, Y. Srebro, and C. Stoeckl, *Phys. Plasmas* **12**, 056307 (2005).
28. R. C. Malone, R. L. McCrory, and R. L. Morse, *Phys. Rev. Lett.* **34**, 721 (1975).
29. R. Epstein, *J. Appl. Phys.* **82**, 2123 (1997).
30. P. Y. Chang, R. Betti, B. K. Spears, K. S. Anderson, J. Edwards, M. Fatenejad, J. D. Lindl, R. L. McCrory, R. Nora, and D. Shvarts, *Phys. Rev. Lett.* **104**, 135002 (2010); R. Betti, P. Y. Chang, B. K. Spears, K. S. Anderson, J. Edwards, M. Fatenejad, J. D. Lindl, R. L. McCrory, R. Nora, and D. Shvarts, *Phys. Plasmas* **17**, 058102 (2010).
31. R. Betti, presented at the 24th IAEA Fusion Energy Conference, San Diego, CA, 8–13 October 2012.
32. T. C. Sangster, V. N. Goncharov, R. Betti, P. B. Radha, T. R. Boehly, D. T. Casey, T. J. B. Collins, R. S. Craxton, J. A. Delettrez, D. H. Edgell, R. Epstein, C. J. Forrest, J. A. Frenje, D. H. Froula, M. Gatu-Johnson, V. Yu. Glebov, D. R. Harding, M. Hohenberger, S. X. Hu, I. V. Igumenshchev, R. T. Janezic, J. H. Kelly, T. J. Kessler, C. Kingsley, T. Z. Kosc, J. P. Knauer, S. J. Loucks, J. A. Marozas, F. J. Marshall, A. V. Maximov, R. L. McCrory, P. W. McKenty, D. D. Meyerhofer, D. T. Michel, J. F. Myatt, R. D. Petrasso, S. P. Regan, W. Seka, W. T. Shmayda, R. W. Short, A. Shvydky, S. Skupsky, J. M. Soures, C. Stoeckl, W. Theobald, V. Versteeg, B. Yaakobi, and J. D. Zuegel, "Improving Cryogenic DT Implosion Performance on OMEGA," submitted to *Physics of Plasmas*.
33. F. J. Marshall, J. A. Delettrez, R. Epstein, R. Forties, R. L. Keck, J. H. Kelly, P. W. McKenty, S. P. Regan, and L. J. Waxer, *Phys. Plasmas* **11**, 251 (2004).
34. F. J. Marshall, J. A. Delettrez, R. Epstein, R. Forties, V. Yu. Glebov, J. H. Kelly, T. J. Kessler, J. P. Knauer, P. W. McKenty, S. P. Regan, V. A. Smalyuk, C. Stoeckl, J. A. Frenje, C. K. Li, R. D. Petrasso, and F. H. Séguin, *Bull. Am. Phys. Soc.* **48**, 56 (2003).
35. O. Morice, *Opt. Eng.* **42**, 1530 (2003).